Int. J. Electrochem. Sci., 13 **(2018)** 6373 – 6387, doi: 10.20964/2018.07.34

International Journal of ELECTROCHEMICAL SCIENCE
www.electrochemsci.org

Electrochemical Performance Evaluations of Spinel $LiAl_{0.15}Mn_{1.85}O_4$ Cathode Materials Prepared by a Solution Combustion Technique for Lithium-Ion Batteries

Jintao Liu[1,2,3], *Hongli Bai*[1,2,3], *Junming Guo*[1,2,3,*], *Changwei Su*[1,2,3], *Xiaofang Liu*[1,2,3]

[1] Key Laboratory of Comprehensive Utilization of Mineral Resources in Ethnic Regions, Yunnan Minzu University, Kunming 650500, *PR* China
[2] Key Laboratory of Resource Clean Conversion in Ethnic Regions, Education Department of Yunnan, Yunnan Minzu University, Kunming 650500, *PR* China
[3] Joint Research Centre for International Cross-border Ethnic Regions Biomass Clean Utilization in Yunnan, Yunnan Minzu University, Kunming 650500, PR China
[*]E-mail: guojunming@tsinghua.org.cn

Received: 4 April 2018 / *Accepted:* 6 May 2018 / *Published:* 5 June 2018

$LiAl_{0.15}Mn_{1.85}O_4$ cathode materials have been rapidly synthesized by a solution combustion technique at various heat treatment time to investigate the crystal morphological change and evaluate the electrochemical performances. The structures of as-prepared samples were characterized by X-ray diffraction (XRD), which demonstrates that all the samples present the typically characteristic diffraction peaks of spinel $LiMn_2O_4$. The crystal morphological changes of the samples were observed by field emission scanning electron microscope (FESEM), which confirms that with the increase of heat treatment time, crystal morphology gradually grows to regular octahedron morphology, the average particle size becomes bigger, homogeneity of particle size distribution increases and agglomeration phenomenon is alleviated. Galvanostatic charge-discharge tests show that $LiAl_{0.15}Mn_{1.85}O_4$ sample sintered at 9 h exhibits the optimal cycling stability and rate performance, which delivers a capacity retention rate of 84.3 % after 500 cycles with an initial discharge specific capacity of 110.5 mAh g^{-1} at 1 C (1 C=148 mAh g^{-1}) and 25 ℃. At the higher rate of 5 C, a capacity retention rate of 82.1 % can be obtained after 500 cycles with an initial discharge specific capacity 103.2 mAh g^{-1} at 5 C and 25 ℃. The elevated-temperature cycling stability of the sample at calcination of 9 h is also optimal, which shows a capacity retention rate of 90.1 % after 100 cycles with an initial discharge specific capacity of 105.3 mAh g^{-1} at 1 C and 55 ℃. Cyclic voltammetry (CV) and electrochemical impedance spectroscopy (EIS) tests prove that the sample at calcination of 9 h presents the better electrode reversibility, the lowest apparent activation energy, more rapidly charge-transfer and Li^+ diffusion kinetics processes.

Keywords: Solution combustion technique, Crystal morphological growth, Heat treatment time, Spinel $LiAl_{0.15}Mn_{1.85}O_4$, Lithium ion batteries

1. INTRODUCTION

Lithium-ion batteries (LIBs) have been dominated the market of power supply, which due to the wide application in the portable electronic devices, electric vehicles (EVs) and hybrid EVs (HEVs) [1, 2]. Compared with other cathode materials, Spinel $LiMn_2O_4$ has been regarded as one of the most promising cathode materials for Lithium ion batteries (LIBs) due to its abundant manganese resources, low cost, low toxicity, good safety, friendly environment, etc [3, 4]. Unfortunately, spinel $LiMn_2O_4$ cathode material undergoes the poor cycling stability, especially at the elevated-temperature above 55 ℃ [5]. The Jahn-Teller effect, the dissolution of Mn^{2+} into electrolyte because of the disproportional reaction of Mn^{3+}, the subsequent deposition of Mn on the negative electrode and the gradual decomposition of electrolyte solution at the higher voltage region and elevated temperature are contributed to the capacity deterioration [6, 7]. To deal with these drawbacks, a major strategy is bulk doped $LiMn_2O_4$ with Al^{3+} cations [1, 9-10, 12-16, 26, 31], which can effectively enhance its structural stability and meanwhile increase the average valence of Mn [9]. Yi et al. [10] synthesized the spinel $LiAl_xMn_{2-x}O_4$ (x=0, 0.02, 0.06 and 0.1) microspheres via co-precipitation route. The $LiAl_{0.06}Mn_{1.94}O_4$ sample exhibited obviously improved electrochemical performances comparing with the pristine $LiMn_2O_4$.

The electrochemical properties of cathode materials are strongly influenced by their phase crystallinity, purity, morphology, particle size and distribution [11, 20]. The heat treatment time is a crucial factor, which intensely affects the crystallinity, morphology and particle size of cathode materials. Yuan et al. [12] prepared Al-doped $LiAl_xMn_{2-x}O_4$ (x=0.05, 0.1 and 0.15) materials using a room-temperature solid-state grinding reaction followed by calcination at 800 ℃ for different durations (3, 6 and 12 h). The results demonstrated that the crystallinity of products increased with increasing calcination time, but a small amount of Mn_3O_4 impurity was detected in the sample calcined for 12 h. Esaki et al. [17] reported the preparation of a $LiMn_2O_4$ cathode materials with nano inclusions at 800 ℃ for different heat treatment time (0, 0.5, 2, 4, 6, 8 and 12 h), which confirmed that the particle sizes of $LiMn_2O_4$ and that of the nano inclusions increased with the increase of heat treatment time. Zhao et at. [18] synthesized spinel-type $LiMn_{1.90}Mg_{0.05}Si_{0.05}O_4$ cathode materials by a citric acid-assisted sol-gel method and the sintering parameters such as sintering time were investigated. The results proved that the average particle size increased with the expanding of sintering time. Lv et al. [19] introduced the preparation of $LiNi_{0.5}Mn_{1.5}O_4$ cathode materials via a solid-state reaction and as-prepared powders were calcined at 850 ℃ for 8-14 h. The optimized condition at 850 ℃ for 12 h exhibited the best crystallinity, the best particle size distribution as well as the highest capacity and optimal rate performance. It was reported by Lu et al. [20] that a nano structured $LiMn_2O_4$ spinel was prepared by a solution combustion synthesis using urea as a fuel at 700 ℃ for 5, 10, 15 and 20 h. The study found that with an increase in the calcination time, the lattice constants tended to decreased at first and then increased. Galvanostatic cycling tests showed that the heat treated at 700 ℃ for 10 h delivered the optimal electrochemical capabilities. However, to the best of our knowledge, no report is available about the investigation of the relationships of crystal morphological growth and electrochemical performances of spinel $LiMn_2O_4$ by Al doping cathode materials prepared at different heat treatment time via a solution combustion technique using HNO_3 solution as an auxiliary oxidant.

In this work, $LiAl_{0.15}Mn_{1.85}O_4$ cathode materials were rapidly synthesized by a combustion technique for combustion reaction at 500 ℃ for 1 h at first, and then calcined at 700 ℃ for different heat treatment time (3, 6, 9 and 12 h) to investigate the relationships of the crystal morphological growth and electrochemical performances.

2. EXPERIMENTAL

2.1 Preparation of materials

The $LiAl_{0.15}Mn_{1.85}O_4$ cathode materials were rapidly prepared by a solution combustion technique at different heat treatment time. At first, 1.1710 g $LiNO_3$ (AR, Aladdin) was used as lithium resource, 7.7014 g $Mn(CH_3COO)_2{\cdot}4H_2O$ (AR, Aladdin) acted as manganese resource and 0.9558 g $Al(NO_3)_3{\cdot}9H_2O$ (AR, Aladdin) was dopant, which were accurately weighted according to a stoichiometric rate of 1:1.85:0.15 (Li:Mn:Al) with a objective product of 3 g and put into a 300 mL crucible, and then 2 mL HNO_3 (AR, KESHI) solution with a concentration of 6 mol L^{-1} was also added into the crucible and then stirred vigorously at room temperature until formed the uniform dispersed mixture. Then the mixture was removed into an oven at 105℃ maintained for about 15 minutes and continually stirred until the mixture was dissolved entirely and formed an homogeneous reddish solution. Subsequently, the solution was submitted into a muffle furnace for combustion reaction at 500 ℃ for 1 h in an air atmosphere and the fluffy-flaky black product was obtained after cooling off to room temperature and grinded. Next, the grinded product was calcined again at 700 ℃ for different heat treatment time (3, 6, 9, 12 h) in a program-controlled furnace and grinded again after cooling off to room temperature. Finally, the black powders were obtained.

2.2 Characterization of materials

The crystal structure, the phase identification and crystallinity of as-prepared samples were characterized by X-ray diffraction (XRD, D8 ADVANCE, BRUKER) with Cu Kα radiation and the measurement rang was from 10° to 70° with a step size of 0.02° and scan speed of 4° min^{-1} at an operation current of 40 mA and voltage of 40 kV. Lattice parameters of as-synthesized samples were obtained by Jade 5.0 refinement software.The crystal morphological growth, particle size and particle distribution of as-prepared materials was observed by field emission scanning electron microscopy (FE-SEM, NOVA NANOSEM 450, America FEI).

2.3 Electrochemical performance tests

Electrochemical performance tests of as-prepared samples were carried out in CR2025 type coin cells using lithium metal as the anode and the reference electrode. To commence, the working electrodes were fabricated as follows: as-prepared $LiAl_{0.15}Mn_{1.85}O_4$ cathode material powder, polyvinylidene fluoride (PVDF) and conductive carbon black were evenly mixed in a mass ratio of

80:10:10 dissolved in the appropriate volume 1-methyl-3-pyrrolidone (NMP) solvent. The obtained slurry was uniformly coated onto an aluminum foil current collector by a doctor-blade technique, and then dried it at 80 ℃ for 4 h in an oven and succedent punched into circular discs with a diameter of 16 mm. All as-prepared cathode disks were dried again at 120 ℃ in vacuum oven for 12 h prior to assemble cell. The mass of active substance on the per current collector was about 2-3 mg. The CR 2025 coin-type cells were assembled in a dry glove box filled with high purity argon gas with pure Li sheet acted as the negative electrode and counter electrode, Celgard 2320-type membranes as the separator, 1 M $LiPF_6$ dissolved in ethylene carbonate(EC), 1,2-dimethyl carbonate (DMC) and ethyl methyl carbonate (EMC) as the electrolyte (EC, DMC, EMC at a volume ratio of 1:1:1). Galvanostatical charge-discharge tests were proceeded by a Land electric test syetem CT2001A (Wuhan Jinnuo Electronics Co., Ltd.) between 3.0-4.5 V (vs. Li/Li^+) at different charge/discharge C-rates. Three-electrode cells were employed using high purity lithium metal foil as counter electrode and reference electrode to conduct Cyclic voltammogram (CV) and Electrochemical impedance spectroscopy (EIS) measurements by an electrochemical workstation (IM6ex, ZAHNER-elektrik GmbH & Co. KG, Kronach, Germany). CV tests were recorded in a potential region between 3.6 and 4.5 V (vs. Li^+/Li). EIS tests were also performed in a frequency rang from 1.0 Hz to 100 Hz with an AC signal amplitude of 5 mV.

3. RESULTS AND DISCUSSION

3.1 Structure and morphology

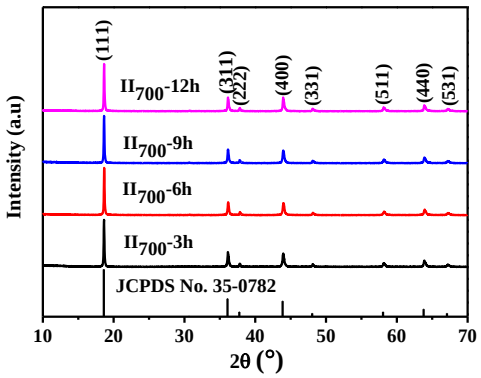

Figure 1. XRD patterns of $LiAl_{0.15}Mn_{1.85}O_4$ samples for the different heat treatment time.

The typical XRD patterns for $LiAl_{0.15}Mn_{1.85}O_4$ samples at 500 ℃ for 1 h and then heat treatment at different time are shown in Fig. 1. It can be seen that all the samples show eight typically characteristic diffraction peaks of (111), (311), (222), (400), (331), (511), (440) and (531), which can be assigned to the well-defined characteristic diffraction peaks of cubic spinel $LiMn_2O_4$ with a space group Fd3m (JCPDS No. 35-0782) [21].

Table 1. The lattice parameters of $LiAl_{0.15}Mn_{1.85}O_4$ samples for the different heat treatment time.

Heat treatment time (h)	Lattice constant (Å)	Cell volume ($Å^3$)	FWHM of (400) peak (°)	$I_{(311)}/I_{(400)}$
3	8.2335	556.12	0.324	1.02
6	8.2334	556.10	0.323	1.09
9	8.2222	555.86	0.319	1.12
12	8.2214	555.69	0.292	1.08

It is noted that the diffraction peak of (220) at around 2θ=30.7° can not be detected in the XRD patterns, which demonstrates that 8a tetrahedral sites are only occupied by Li^+ ion, the 16d octahedron sites of the cubic close-packed O^{2-} structure are entirely occupied by Mn^{3+} ion, Mn^{4+} ion and doping Al^{3+} ion [22], Al doping does not change the intrinsic spinel structure, but to successfully enter the lattice of spinel $LiMn_2O_4$. The XRD data were fitted by Rietveld refinement software to obtain the lattice parameters of $LiAl_{0.15}Mn_{1.85}O_4$ sample for the different heat treatment time and relevant data are listed in Table 1. It can be seen from the Table 1, with the increase of heat treatment time, both lattice constant and cell volume tend to decrease, which indicate that increasing the calcination time cause structural shrinkage. Moreover, the full width at half-maximum (FWHM) became slightly smaller as the increase of calcination time, which implies that increasing the heat treatment time can enhance the crystallinity of grain. Besides, the ratio of $I_{(311)}/I_{(400)}$ peaks tends to increase firstly and then decline, and the calcination time at 9 h shows the highest ratio of $I_{(311)}/I_{(400)}$ peaks, which suggests its better electrochemical performance.

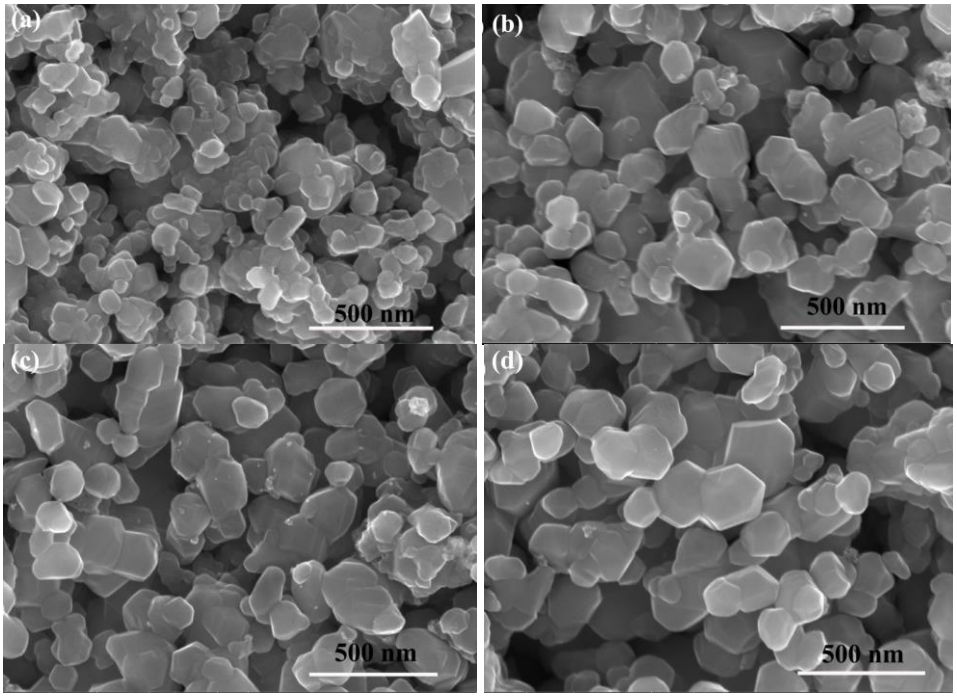

Figure 2. SEM images of $LiAl_{0.15}Mn_{1.85}O_4$ samples at 700 ℃ for the different heat treatment time (a) 3 h, (b) 6 h, (c) 9 h and (d) 12 h

Fig. 2 exhibits the SEM images of samples at 700 ℃ for the different heat treatment time. It can be seen from Fig. 2 that all the samples are made up of sub-micron sized particles in the rang of 100-300 nm. What is more, the average particle size of prepared samples becomes bigger with the enhancing of heat treatment time, crystal morphology gradually grows to regular octahedron morphology, the outline and boundary of octahedron crystal become more and more clearer, particle size distribution becomes more homogeneous and the agglomerate phenomenon of particles can be gradually alleviated. The results indicate that enhancing the calcination time can effectively facilitate the nucleation rate, equalize the size distribution and suppress the agglomerate of particles.

3.2 Cyclic stability and rate capacity

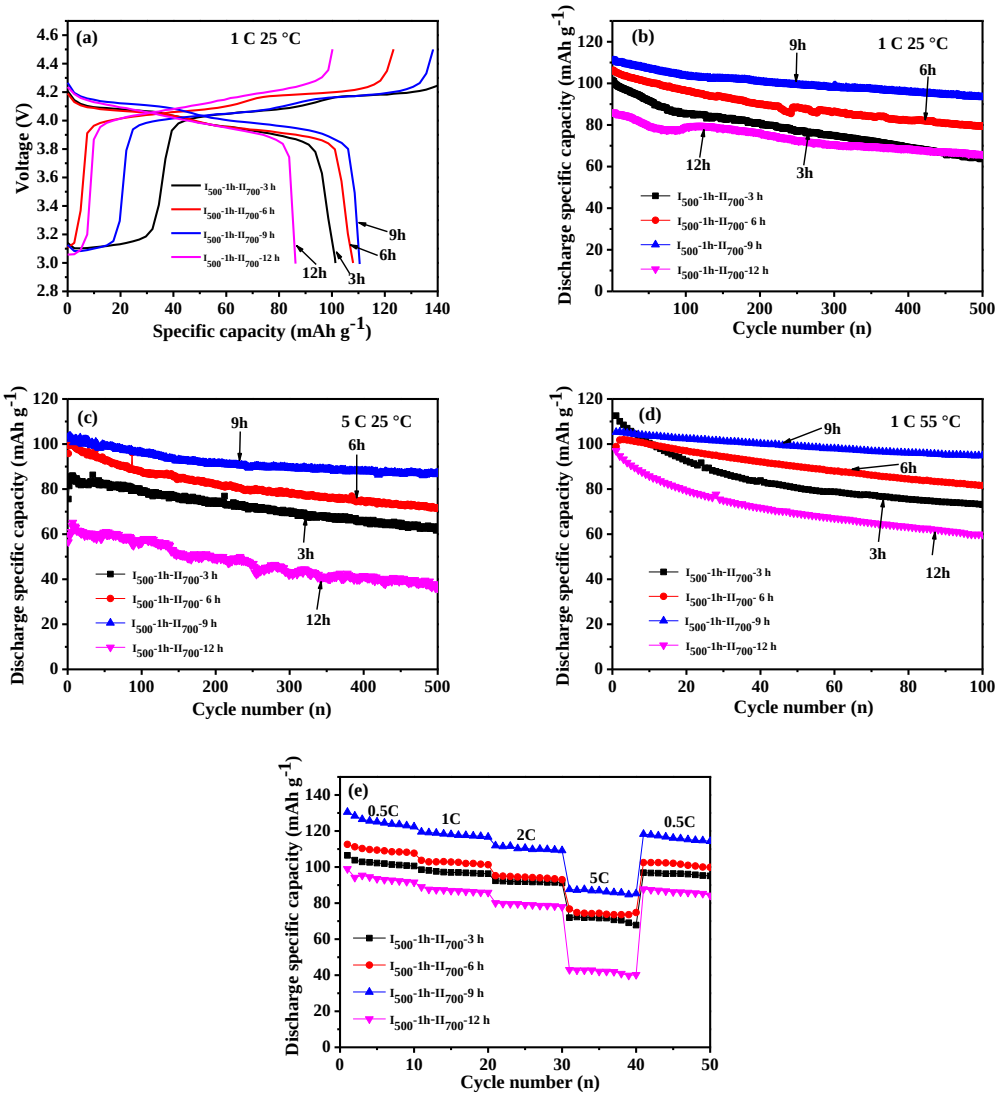

Figure 3. (a) initial charge-discharge curves of $LiAl_{0.15}Mn_{1.85}O_4$ samples at the different heat treatment time at 1 C and 25 ℃. The cyclic performances of $LiAl_{0.15}Mn_{1.85}O_4$ samples at the different heat treatment time: (b) at 1 C, (c) at 5 C and 25 ℃, (d) at 1 C and 55 ℃, (e) the rate performances of $LiAl_{0.15}Mn_{1.85}O_4$ samples at the different heat treatment time.

In order to investigate the relationship between crystal morphology growth and cycling performances, galvanostatic charge-discharge cycling performance and rate performance tests were carried out at 25 and 55 ℃. Fig. 3 (a) displays the first galvanostatic charge-discharge profiles of the samples at the different calcination time at 1 C rate and in the voltage window of 3.0-4.5 V. Two apparent potential plateaus can be seen in all samples at about 4.0 V and 4.1 V, suggesting the typically well-define spinel $LiMn_2O_4$ during two-stage Li^+ ion insertion and extraction processes [23], relating to the two-phase conversion of $MnO_2/Li_{0.5}Mn_2O_4$ at about 4.0-4.1 V vs. Li/Li^+ and $Li_{0.5}Mn_2O_4/LiMn_2O_4$ at about 3.9-4.0 V vs. Li/Li^+ [24]. It can be found that the initial discharge specific capacity of as-prepared samples tend to increase firstly and then decrease with the increase of heat treatment time. The cycle performances of the samples at different calcination time at 1 C and 5 C rates at 25 ℃ are shown in Fig. 3 (b) and (c), respectively, and the relevant data are summarized in Table 2. Regardless of at 1 C and 5 C rates, the cycling capabilities of as-prepared samples follow the order: 9 h >6 h > 3 h > 12 h. As exhibited in Table 2, among these samples prepared at various calcination time, the sample prepared at 9 h delivers optimal discharge specific capacities and capacity retention rates. Especially, the sample prepared at 9 h displays a excellent discharge specific capacity of 87 mAh g^{-1} with a capacity retention rate of 82.3 % at 5 C and 25 ℃ after 500 cycles, while the sample prepared at 12 h only provides a discharge specific capacity of 36 mAh g^{-1} with a capacity retention rate of 63.7 % at the same conditions.

Table 2. Discharge specific capacity and capacity retention rate of $LiAl_{0.15}Mn_{1.85}O_4$ samples at the different heat treatment time at 25 ℃.

Heat treatment time (h)	1 C Discharge capacity (mAh g^{-1})		Capacity retention rate (%)	5 C Discharge capacity (mAh g^{-1})		Capacity retention rate (%)
	Initial	500^{th}		Initial	500^{th}	
3	101.6	63.9	62.9	75.6	63.3	83.7
6	106.3	79.4	74.7	95.8	71.6	74.7
9	110.5	93.2	84.3	103.2	84.7	82.1
12	86.2	66	76.6	56.5	36	63.7

Table 3. Discharge specific capacity and capacity retention rate of $LiAl_{0.15}Mn_{1.85}O_4$ samples at the different heat treatment time at 1 C rate and 55 ℃.

Heat treatment time (h)	Discharge capacity (mAh g^{-1})		Capacity retention rate (%)
	Initial	100^{th}	
3	112.6	73.1	65
6	98.9	81.6	82.5
9	105.3	94.9	90.1
12	97	60	61.8

The elevated-temperature cycling stability of as-synthesized samples also was evaluated at 1 C and 55 ℃, the measurement results are showed in Fig. 3 (d) and the relevant data are listed in Table 3.

The same phenomenon can be found that the sample prepared at 9 h takes on the optimal cycling stability compared with the samples prepared at other calcination time. It delivers a discharge specific capacity of 94.9 mAh g^{-1} with a capacity retention rate of 90.1 % after 100 cycles, which is obviously higher than other samples.

Fig. 3 (e) shows the reversible discharge specific capacities as a function of C-rate for as-prepared samples at different heat treatment time. It can be seen that the discharge specific capacities of all products decrease gradually with the increase of current density due to the effect of electrochemical polarization and ohmic polarization, restricting the Li^+ diffusion rate in spinel structure [25]. Nevertheless, The sample prepared at heat treatment time of 9 h presents better rate performance than the samples prepared at other heat treatment time. Even at higher rate of 5 C, the discharge specific capacity for the sample at calcination of 9 h can achieve up to about 98 mAh g^{-1}. When the rates decrease from 5 C to 0.5 C, its initial discharge specific capacity can be recovered, which indicates that it has better electrochemical reversibility. The excellent cycling and rate performances can be ascribed to the reasons that Al-doping can suppress the Jahn-Teller distortion, moderately increasing the heat treatment time can enhance the crystallinity of grains, contribute to the growth of particles and homogenize the distribution of particles. The well-developed crystals are in favor of restraining dissolution of Mn^{2+} into the electrolyte, alleviating deposition of Mn on the negative electrode and shortening the Li^+ migration path. We also made a comparison with similar cathode materials that were described in references including our work, as summarized in Table 4. A remarkable conclusion can be made that the electrochemical performance of as-prepared materials by the solution combustion technique is comparable to those reported.

Table 4. Comparison of the similar cathode materials described in the references including our work.

Material	Preparation method	Initial capacity and capacity retention	Ref.
$LiMn_{1.90}Al_{0.10}O_4$	Self-template	110 mAh g^{-1}, 80% after 200 cycles at 5C and 55℃	9
$LiAl_{0.06}Mn_{1.94}O_4$	Co-precipitation	117.4 mAh g^{-1}, 97% after 100 cycles at 1C and 55℃	10
$LiMn_{1.85}Al_{0.15}O_4$	Solid-State reaction	117 mAh g^{-1}, 97.9% after 50 cycles at 1C and 25 ℃	13
$LiAl_{0.1}Mn_{1.9}O_4$	Phase-inversion	120 mAh g^{-1}, 85% after 50 cycles at 1C and 55 ℃	14
$LiAl_{0.08}Mn_{1.92}O_4$	Polymer-pyrolysis	116.2 mAh g^{-1}, 99.3% after 50 cycles at 55℃	15
$LiAl_{0.04}Mn_{1.96}O_4$	Solid-state combustion reaction	108.4 mAh g^{-1}, 90.3% after 50 cycles at 0.2C and 25℃	16
$LiAl_{0.1}Mn_{1.9}O_4$	Template-engaged method	90 mAh g^{-1}, 70% after 500 cycles at 3C and 50 ℃	26
$LiAl_{0.1}Mn_{1.9}O_4$	Solid-phase reaction	121.2 mAh g^{-1}, 95% after 100 cycles at 0.2C and 25℃	31
$LiAl_{0.15}Mn_{1.85}O_4$	Solution combustion	105.3 mAh g^{-1}, 90.1% after 100 cycles at 1C and 55℃	This work

3.3 Cyclic voltammetry

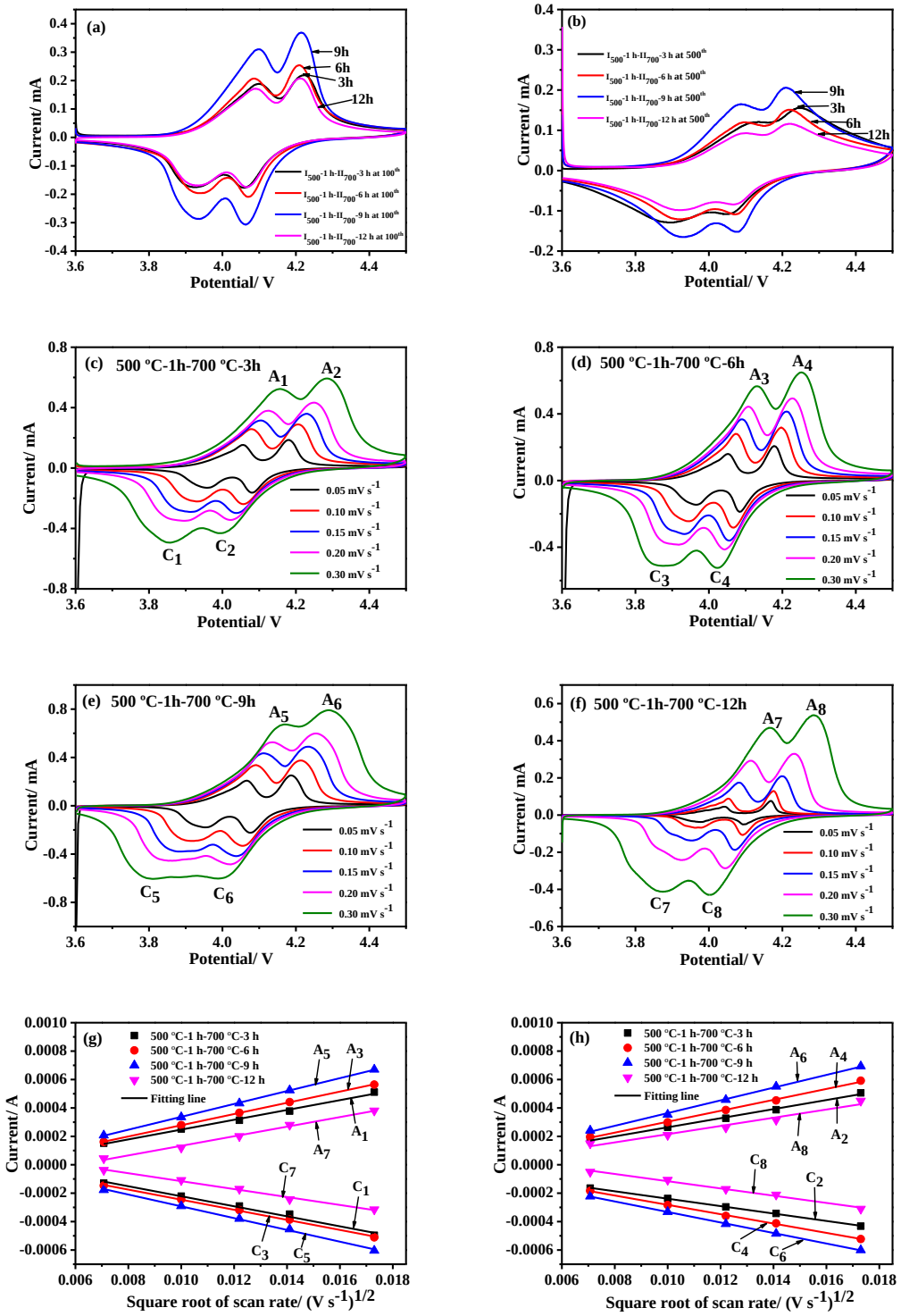

Figure 4. CV curves of $LiAl_{0.15}Mn_{1.85}O_4$ samples at the different heat treatment time (a) after 100 cycles and (b) after 500 cycles at 1 C rate and 25 °C in the potential rang of 3.6-4.5 V (vs. Li/Li^+) at a scan rate of 0.1 mV s^{-1}. CV curves of (c)-(f) $LiAl_{0.15}Mn_{1.85}O_4$ samples at the different heat treatment time in the potential rang of 3.6-4.5 V (vs. Li/Li^+) at different scan rates from 0.05 to 0.30 mV s^{-1}, (g) and (h) plots of peak current vs. square root of the scan rate for $LiAl_{0.15}Mn_{1.85}O_4$ samples at the different heat treatment time.

In order to elucidate electrochmical cycling reversibility of as-synthesized materials [26], CV measurements were conducted for the electrodes after 100 and 500 cycles in the potential rang of 3.6-4.5 V (vs. Li/Li^+) at a scan rate of 0.1 mV s^{-1}, and the results are shown in Fig. 4 (a) and (b), respectively. It is distinct that either after 100 or 500 cycles, all the CV curves exhibits two couples of redox peaks, which can be assigned to two steps processes of intercalation/ extraction of Li^+ ion into/ from the spinel phase and correspond to two charge-discharge potential plateaus showed in Fig. 3(a) [27, 28]. After 100 cycles, all of the CV curves display two pairs of well separated and symmetric redox peaks, however, with the cycling going on, especially after 500 cycles, the anodic peaks shift to more positive potential and the cathodic peaks shift to more negative potential, resulting in the larger potential difference (ΔE) of two anodic and cathodic peaks. It can be seen from the CV curves, the cathode material prepared at calcination time of 9 h displays the smaller potential difference (ΔE) and higher current of redox peaks, well separated and more symmetric redox peaks than other samples, in spite of after 100^{th} cycles or 500^{th} cycles. Therefore, the electrode prepared for calcination of 9 h shows the smaller electrochemical polarization, the better electrochemical reversibility and activity [29].

Table 5. Li^+ diffusion coefficient of as-prepared electrodes at different heat treatment time.

Heat treatment time (h)	Peaks	Li^+ diffusion coefficient, D ($cm^2 \cdot s^{-1}$)
3	A_1	7.22×10^{-12}
	A_2	6.18×10^{-12}
6	A_3	9.43×10^{-12}
	A_4	8.95×10^{-12}
9	A_5	1.24×10^{-11}
	A_6	1.21×10^{-11}
12	A_7	6.88×10^{-12}
	A_8	5.06×10^{-12}

In order to investigate the kinetic process of electrodes, a series of the CV tests of as-prepared electrodes at different heat treatment time were proceeded in the potential rang of 3.6-4.5 V (vs. Li/Li^+) at various scan rates from 0.05 to 0.30 mV s^{-1} and the results are depicted in Fig. 4 (c)-(f). It is reported that the rate performance of material is strongly dominated by its Li^+ diffusion rate, and Li^+ diffusion rate is directly determined by Li^+ diffusion coefficient (D_{Li}). Li^+ diffusion coefficient (D_{Li}) can be calculated by the following equation [30]:

$$i_p = (2.69\times10^5)n^{3/2}C_{Li}AD_{Li}^{1/2}v^{1/2} \quad (25\ ^\circ C) \qquad (1)$$

In the equation 1, i_p is the peak current (A) of redox peaks, n stands for the charge-transfer number (n≈1 for spinel $LiMn_2O_4$), C_{Li} is the bulk concentration of Li^+ in the electrode (given as 0.02378 mol cm^{-3} for spinel $LiMn_2O_4$ dated from the theoretical density of 4.3 g cm^{-3}), A is the surface area of the electrode (cm^2), D_{Li} is the Li^+ diffusion coefficient (cm^2 s^{-1}) and *v* represents the scan rate (V s^{-1}). The plots of the peak current vs. square root of the scan rate for as-prepared electrodes also are given in Fig. 4 (g) and (h). According to the fitting results, the peak currents (i_p) and square root of the scan rates ($v^{1/2}$) display favourable linear relationships, which indicates that intercalation reaction is

kinetically controlled by solid-state diffusion of Li^+ [31]. The Li^+ diffusion coefficients of electrodes are calculated on the basis of the slopes of linear fitting and constants in the Eq. 1, which are listed in Table 4. It can be found that Li^+ diffusion coefficients of as-prepared sample at calcination time of 9 h are larger than that of other samples, demonstrating the faster Li^+ diffusion kinetics of as-prepared sample at calcination time of 9 h, which well corresponds to its optimal rate performance.

3.4 Electrochemical impedance spectroscopy

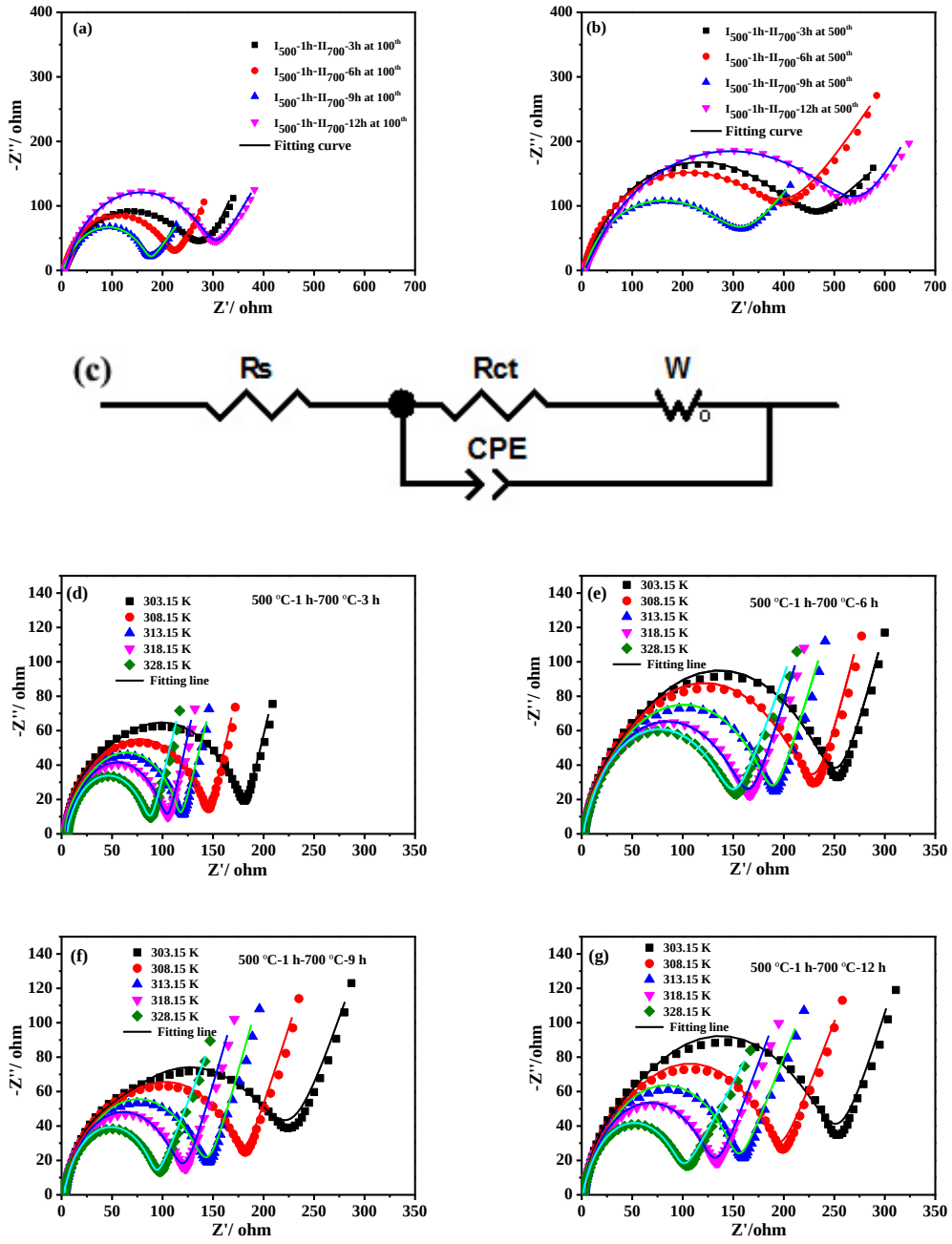

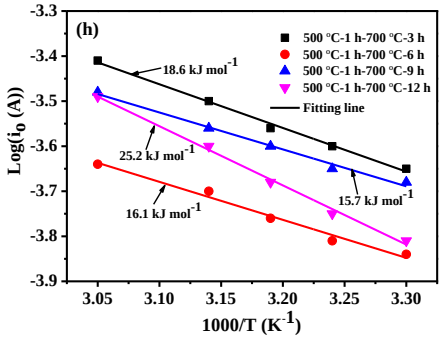

Figure 5. Nyquist plots of $LiAl_{0.15}Mn_{1.85}O_4$ samples at the different calcination time (a) after 100 cycles and (b) after 500 cycles at 1 C rate and 25 °C, (c) the equivalent circuit model. Nyquist plots of (d)-(g) $LiAl_{0.15}Mn_{1.85}O_4$ samples at the different calcination time at different temperatures and (h) Arrhenius plots of log i_0 vs. 1/T for $LiAl_{0.15}Mn_{1.85}O_4$ samples at the different heat treatment time.

In order to explore the electrode processes, EIS measurements were analyzed. Fig. 5 (a) and (b) show Niquist plots of $LiAl_{0.15}Mn_{1.85}O_4$ samples prepared at the different heat treatment time after 100 and 500 cycles at 1C rate and 25 °C. It can be clearly seen that all Niquist plots are primarily consisted of three parts, namely the intercept at the real axis (Z′) in the high frequency region, the semicircle at high to middle frequency region and a sloping line in the low frequency zone. The intercept stands for ohmic resistance (R_s) of electrolyte. The semicircle represents the charge transfer resistance (R_{ct}), which derives from charge transfer reaction between surface film and spinel particles, which is strongly linked with the electrochemical properties of as-prepared samples [32]. The inclined line is attributed to Warburg impedance (W), which reflects the Li^+ diffusion in the bulk electrode [33, 34]. The equivalent circuit model was depicted in Fig. 5 (c), which is used for fitting EIS data, wherein the constant phase element (CPE) is the double layer capacitance. The fitting values of R_{ct} are listed in Table 5. As showed in Table 5, the values of R_{ct} tend to reduce firstly and then increase with the increase of heat treatment time, and the sample prepared at calcination of 9 h gives the lowest R_{ct} values, whether after 100 or 300 cycles. The above results prove that the sample prepared at calcination of 9 h exhibits more rapid charge transfer kinetics [35].

Table 6. The fitting values of R_{ct} obtained from the equivalent circuit model.

Heat treatment time (h)	Fitting values of R_{ct} (Ω)	
	100^{th}	500^{th}
3	225.6	391.0
6	196.1	331.6
9	158.0	250.0
12	261.7	500.3

A series of EIS tests also were carried out at various temperatures to further understand the electrode kinetics and calculate the apparent activation energies (E_a). Fig. 5 (d)-(g) illustrate the Nyquist plots of as-synthesized samples at various heat treatment time and different temperatures. The apparent activation energies (E_a) of the electrodes can be calculated by the following equations [36]:

$$i_0 = RT / nFR_{ct} \quad (2)$$

$$i_0 = A\exp(-E_a / RT) \quad (3)$$

In the equations, i_0 represents the exchange current, R stands for the gas constant (8.314 J mol^{-1} K^{-1}), T (K) is the absolute temperature, n is the number of charge-transfer ($n\approx1$ for spinel $LiMn_2O_4$), F is the Faraday constant (96484.5 C mol^{-1}). R_{ct} is charge transfer resistance, which can be obtained by fitting using the same equivalent circuit model showed in Fig. 5 (c), A is a temperature-independent coefficient. Fig. 5 (h) gives the Arrhenius plots of log i_0 as a function of 1/T of as-prepared electrodes. On the basis of the eq. 2 and eq. 3, the transformed equation of the apparent activation energy (E_a) can be expressed: Ea=-Rkln10, wherein k is the slope of the fitting line. According to the values of slopes of the fitting lines, the values of E_a of as-synthesized samples at various heat treatment time of 3, 6, 9 and 12 h are 18.6, 16.1, 15.7 and 25.2 kJ mol^{-1}, respectively. With the increase of calcination tome, the values of E_a tends to decrease firstly and then subsequently increase. It is worth noticing that as-prepared sample at heat treatment time of 9 h reveals the lowest values of E_a among these samples, which attests the shorter Li^+ diffusion path of the sample synthesized at calcination of 9 h, meaning its better electrochemical performance [37], which can be ascribed to its uniform particle distribution and moderate particles size.

4. CONCLUSIONS

In summary, this work reported that we investigated the relationships of the crystal morphological change and electrochemical performances by spinel $LiAl_{0.15}Mn_{1.85}O_4$ cathode materials prepared at different heat treatment duration via a solution combustion technique. It was confirmed that as the increase of calcination time, both lattice constant and cell volume tended to shrink. Moreover, with the increase of sintering time, the crystallinity of the samples enhanced, particle size became bigger, crystal morphology gradually developed to regular octahedrons morphology, agglomeration phenomenon of particles was relieved to some extent and the size distribution of particles became more homogeneous. Among these as-prepared compounds, the $LiAl_{0.15}Mn_{1.85}O_4$ sample at calcination of 9 h exhibited the optimal electrochemical properties, which achieved up to a capacity retention rate of 84.3 % after 500 cycles with an initial discharge specific capacity of 110.5 mAh g^{-1} at 1 C and 25 ℃. When tested at 5 C and 25 ℃, an initial discharge specific capacity of 103.2 mAh g^{-1} could be achieved with a capacity retention rate of 82.1 % after 500 cycles. Meanwhile, the sample at sintering time of 9 h also showed much superior elevated-temperature cycling stability, which reached up to an initial discharge specific capacity of 105.3 mAh g^{-1} at 1 C and 55 ℃ and the capacity retention rate of 90.1 % was preserved after 100 cycles, which were much better than that of other samples. The obviously enhanced electrochemical performances can be ascribed to the reasons

that the sample at an appropriate heat treatment time by a solution combustion method displayed the good crystallinity, uniform size distribution of particles, higher Li^+ coefficient, lower charge transfer resistance and apparent activation energy.

ACKNOWLEDGMENTS
This work was financially supported by the National Natural Science funds projects of China (51462036, U1602273).

References

1. Y. Fu, H. Jiang, Y. J. Hu, Y. H. Dai, L. Zhang, and C. Z. Li, *Ind. Eng. Chem. Res*., 54 (2015) 3800-3805.
2. X. Yi, X. Y. Wang, B. W. Ju, H. B. Shu, W. C. Wen, R. Z. Yu, D. Wang, X. K. Yang, *Electrochim. Acta*, 134 (2014) 143-149.
3. D. Tang, Y. Sun, Z. Yang, L. Gu and X. Huang, *Chem. Mater*., 26 (2014) 3535-3543.
4. C. H. Zheng, Z. F. Wu, J. C. Li, X. Liu, D. L. Fang, *Ceram. Int*., 40 (2014) 8455-8463.
5. J. Molenda, M. Ziemnicki, J. Marzec, W. Zaj, M. Molenda, *J. Power Sources*, 173 (2007) 707-711.
6. T. F. Yi, Y. Xie, Y. R. Zhu, R. S. Zhu and M. F. Ye, *J. Power Sources*, 211 (2012) 59-65.
7. D. H. Jang, Y. J. Shin, S. M. Oh, *J. Electrochim. Sci*., 143 (1996) 2204.
8. D. W. Han, W. H. Ryu, W. K. Kim, J. Y. Eom, and H. S. Kwon, *J. Phys. Chem*. C, 117 (2013) 4913-4919.
9. Y. L. Ding, J. Xie, G. S. Gao, T. J. Zhu, H. M. Yu, and X. B. Zhao, *J. Phys. Chem*. C, 115 (2011) 9821-9825.
10. X. Yi, X. Y. Wang, B. W. Ju, Q. L. Wei, X. K. Yang, G. S. Zou, H. B. Shu, L. Hu, *J. Alloys Compd.*, 604 (2014) 50-56.
11. Y. J. Cai, Y. D. Huang, X. C. Wang, D. Z. Jia, X. C. Tang, *Ceram. Int*., 40 (2014) 14039-14043.
12. A. B. Yuan, L. Tian, W. M. Xu, Y. Q. Wang, *J. Power Sources*, 195 (2010) 5032-5038.
13. X. Y. Feng, Y. Tian, J. X. Zhang, L. W. Yin, *Powder Technol*., 253 (2014) 35-40.
14. J. L. Wang, Z. H. Li, J. Yang, J. J. Tang, J. J. Yu, W. B. Nie, G. T. Lei, Q. Z. Xiao, *Electrochim. Acta*, 75 (2012) 115-122.
15. L. F. Xiao, Y. Q. Zhao, Y. Y. Yang, Y. L. Cao, X. P. Ai, H. X. Yang, *Electrochim. Acta*, 54 (2008) 545-550.
16. C. C. Peng, J. J. Huang, Y. J. Guo, Q. L. Li, H. L. Lai, Y. H. He, C. W. Su, J. M. Guo, *Vacuum*, 120 (2015) 121-126.
17. Shogo Esaki, Motoaki Nishijima, Shigeomi Takai and Takeshi Yao, *RSC Adv*., 5 (2015) 42455-42460.
18. H. Y. Zhao, X. Q. Liu, C. Cheng, Z. Zhang, Y. Wu, B. Chen, W. Q. Xiong, *J. Solid State Electrochem.*, 19 (2015) 1015-1026.
19. Y. Z. Lv, Y. Z. Jin, Y. Xue, J. Wu, X. G. Zhang and Z. B. Wang, *RSC Adv*., 4 (2014) 26022-26029.
20. C. Z. Lu, George Ting-Kuo Fey, *J. Phys. Chem. Solids*, 67 (2006) 756-761.
21. Y. Wang, Q. Peng, G. Yang, Z. Yang, L. C. Zhang, H. Long, Y. H. Huang, P. X. Lu, *Electrochim. Acta*, 136 (2014) 450-456.
22. H. Y. Zhao, F. Li, X. Q. Liu, C. Cheng, Z. Zhang, Y. Wu, W. Q. Xiong, B. Chen, *Electrochim. Acta*, 151 (2015) 263-269.
23. D. Arumugam, G. Paruthimal Kalaignan, *J. Electroanal. Chem*., 648 (2010) 54-59.
24. L. F. Duan, X. Y. Zhang, K. Q. Yue, Y. Wu, J. Zhuang and W. Lü, *Nanoscale Res. Lett*., 12 (2017) 109.

25. J. Wang, Y. Y. Yu, B. H. Wu, W. Q. Lin, J. Y. Li and J. B. Zhao, *J. Mater. Chem*. A, 3 (2015) 2357.
26. D. Zhan, Y. Liang, P. Cui and Z. A. Xiao, *RSC Adv*., 5 (2015) 6372-6377.
27. B. S. Qin, Z. H. Liu, G. L. Ding, Y. L. Duan, C. J. Zhang, G. L. Cui, *Electrochim. Acta*, 141 (2014) 167-172.
28. H. L. Zhang, L. Zhang, S. W. Yang, *J. Electrochem. Sci.*, 9 (2014) 8182-8188.
29. B. W. Ju, X. Y. Wang, C. Wu, X. K. Yang, H. B. Shu, Y. S. Bai, W. C. Wen, X. Yi, *J. Alloys Compd.*, 584 (2014) 458.
30. Y. Z. Wang, X. Shao, H. Y. Xu, M. Xie, S. X. Deng, H. Wang, J. B. Liu, H. Yan, *J. Power Sources*, 226 (2013) 145-146.
31. D. L. Guo, B. Li, Z. R. Chang, H. W. Tang, X. H. Xu, K. Chang, E. B. Shangguan, X. Z. Yuan, H. J. Wang, *Electrochim. Acta*, 134 (2014) 338-346.
32. L. Xiong, Y. Xu, C. Zhang, Z. Zhang, J. Li, *J. Solid State Electrochem*., 15 (2011) 1263-1269.
33. D. L. Fang, J. C. Li, X. Liu, P. F. Huang, T. R. Xu, M. C. Qian, C. H. Zheng, *J. Alloys Compd*., 640 (2015) 82-89.
34. M. W. Xiang, C. W. Su, L. L. Feng, M. L. Yuan, J. M. Guo, *Electrochim. Acta*, 125 (2014) 524-529.
35. H. Y. Zhao, X. Q. Liu, C. Cheng, Q. Li, Z. Zhang, Y. Wu, B. Chen, W. Q. Xiong, *J. Power Sources*, 282 (2015) 118-128.
36. S. L. Chou, J. Z. Wang, H. K. Liu, and S. X. Dou, *J. Phys. Chem*. C, 115 (2011) 16225.
37. S. L. Chou, J. Z. Wang, J. Z. Sun, David Wexler, Maria Forsyth, H. K. Liu, Douglas R. MacFarlane, and S. X. Dou, *Chem. Mater*. 20 (2008) 7050-7051.